MINISTRY OF EDUCATION AND TRAINING

VIETNAM ACADEMY OF SCIENCE AND TECHNOLOGY

GRADUATE UNIVERSITY OF SCIENCE AND TECHNOLOGY

Vu Anh Tuan

A STUDY OF PIEZOELECTRIC STACK ENERGY HARVESTER IN THE LINEAR SYSTEM WITH TWO DEGREES OF FREEDOM

SUMMARY OF DISSERTATION ON MECHANICAL ENGINEERING AND ENGINEERING MECHANICS

Major: Engineering Mechanics

Code: 9 52 01 01

Hanoi - 2024

The dissertation is completed at: Graduate University of Science and Technology, Vietnam Academy Science and Technology.

Supervisor 1: Prof. Nguyen Dong Anh
Supervisor 2: Dr. Nguyen Ngoc Linh

Referee 1:.....
Referee 2:.....
Referee 3:.....

The dissertation is examined by Examination Board of Graduate University of Science and Technology, Vietnam Academy of Science and Technology at ……..

The dissertation can be found at:

1. Graduate University of Science and Technology Library
2. National Library of Vietnam

INTRODUCTION

1. The reason for choosing the topic of the study

In recent decades, research in the field of energy harvesting to eliminate the wasted energy available in the surrounding environment, such as vibration, heat, light, radiation, wind and water, into electrical energy to replace the use of power from the grid or batteries for low-power electronic devices for sensors or measuring devices used in vehicles, construction equipment or artificial biological parts has been receiving attention from many researchers.

One of the wasted energy sources that can be harvested for many different applications is vibration from the surrounding environment.

Many designs and approaches have been proposed to convert mechanical energy from vibration sources in the environment into electrical energy for small and micro-power electronic devices. Among them, the piezoelectric mechanism has many wide applications, from energy harvesting devices (piezoelectric energy harvester, PEH), to sensors or actuators.

The piezoelectric stack energy harvester (PSEH) is composed of many layers of piezoelectric ceramics installed in series, between them are electrodes, these electrodes are connected to an external resistor (load). With such structural characteristics, PSEH allows to reduce the distance between the electrodes and thereby increase the efficiency of energy collection when mechanically deformed compared to a piezoelectric block of the same size. In addition, PSEH is also capable of withstanding large loads, so it can be applied to large structural objects. Some typical applications of PSEH include integration with backpacks, shoes, pavement, vehicle suspension systems, railway tracks, vibration absorbers, etc.

In the period from 2010 onwards, researchers mostly used the 1-degree-of-freedom mechanical model to study applications with piezoelectric energy harvesting devices. The disadvantage of the 1-degree-of-freedom mechanical model is that it only works effectively in the resonance region, leading to low energy harvesting efficiency and not reflecting the reality of vibration sources. Meanwhile, later studies have shown that the 2-degree-of-freedom mechanical system model has a wider effective working frequency range, so it is suitable for vibration sources from the surrounding environment that often have frequencies that vary over time or randomly.

In addition, the integration of vibration damping with electromagnetic energy harvesting from vibration has become increasingly attractive in recent years due to its increasing importance in various real-world applications such as vehicle suspension systems or vibration absorbers. Such a device is called a dual-function device and this research direction is still under development. Therefore, this thesis focuses on the study of a dual-function device which is a tuned mass damper integrated with a piezoelectric stack energy harvester

mounted on an undamped primary structure subjected to harmonic excitation based on a 2-degree-of-freedom mechanical model.

2. The goal of the study

Building a physical model and analysis method, determining parameters as well as evaluating the vibration reduction efficiency combined with energy harvesting of a tuned mass damper integrated with a piezoelectric stack energy harvester mounted on an undamped primary structure subjected to harmonic excitation.

3. The object, scope of the study and research methodology

The object of the study: tuned mass damper integrated with a piezoelectric stack energy harvester.

The scope of the study: The electromechanical parameters of the system include a tuned mass damper integrated with a piezoelectric stack energy harvester mounted on an undamped primary structure under harmonic excitation.

The research methodology: The thesis uses analytical approach to obtain theoretical results which are parameters of the research object. Then conduct numerical examination using Matlab software to illustrate the theoretical results found.

4. Content of the study

The thesis includes an introduction, conclusion, future work, list of published papers related to the thesis, list of references and 4 chapters.

CHAPTER 1. BACKGROUND

In chapter 1, the thesis presents the following issues:

- An overview of piezoelectric materials and applications in vibration energy harvesting for portable and implantable electronic devices as well as self-powered wireless systems and sensors.

- Research on applications of piezoelectric energy harvesting from vibration in linear 2-degree-of-freedom mechanical systems for structures subjected to heavy loads in engineering practice, typically the application direction for vibration absorbers integrated with piezoelectric energy harvesting;

- The research direction chosen for the thesis is the tuned mass damper TMD integrated with a piezoelectric stack energy harvester PSEH mounted on the undamped primary structure subjected to harmonic excitation.

CHAPTER 2. THEORETICAL BASIS FOR CALCULATION OF TUNED MASS DAMPER WITH PIEZOELECTRIC STACK ENERGY HARVESTER

2.1. Tuned Mass Damper

2.1.1. Undamped primary structure under harmonic base excitation

Consider the mechanical system depicted in Figure 2.1, consisting of a tuned mass damper (TMD) attached to an undamped primary structure subjected to harmonic base excitation.

The governing equations for the system:

$$m_1\ddot{x}_1 - c_2\dot{x}_2 + k_1x_1 - k_dx_2 = -m_1\ddot{z} \tag{2.1}$$

$$m_2\ddot{x}_2 + c_2\dot{x}_2 + k_dx_2 = -m_2(\ddot{x}_1 + \ddot{z}) \tag{2.2}$$

By setting: $\mu = \frac{m_2}{m_1}, \omega_1 = \sqrt{\frac{k_1}{m_1}}, \omega_d = \sqrt{\frac{k_d}{m_2}}, \xi = \frac{c_2}{2m_2\omega_d}, \beta = \frac{\omega_d}{\omega_1}, \lambda = \frac{\Omega}{\omega_1}$ (2.3)

where, μ is the ratio of masses, ω_1 is the natural frequency of the primary system, ω_d, ξ, β are the natural frequency, damping and tuning ratios of of TMD, , respectively; λ is the ratio of excitation frequency to primary system's natural frequency.

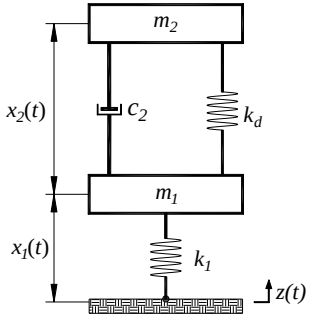

Figure 2.1 Undamped primary system with TMD under harmonic base excitation

The governing equations (2.1)–(2.2) can be rewritten as:

$$\ddot{x}_1 - 2\mu\omega_d\xi\dot{x}_2 + \omega_1^2x_1 - \mu\omega_d^2x_2 = -\ddot{z} \tag{2.4}$$

$$\ddot{x}_2 + 2\omega_d\xi\dot{x}_2 + \omega_d^2x_2 = -\ddot{x}_1 - \ddot{z} \tag{2.5}$$

Applying the fixed-points theory by Den Hartog 1965 for the system (2.4)–(2.5), the optimal tuning and damping ratios of TMD attached to an undamped primary structure subjected to harmonic base excitation are given in the form, respectively:

$$\beta^* = \frac{\sqrt{2+\mu}}{\sqrt{2}(1+\mu)} \tag{2.6}$$

$$\xi^* = \sqrt{\frac{3\mu}{8(1+\mu)}} \tag{2.7}$$

2..1.2. Undamped primary structure under harmonic external excitation

Consider the mechanical system depicted in Figure 2.2, consisting of a tuned mass damper (TMD) attached to an undamped primary structure subjected to harmonic external excitation. The governing equations for the system:

$$m_1\ddot{x}_1 - c_2\dot{x}_2 + k_1x_1 - k_dx_2 = F(t) \tag{2.8}$$

$$m_2\ddot{x}_2 + c_2\dot{x}_2 + k_dx_2 = -m_2\ddot{x}_1 \tag{2.9}$$

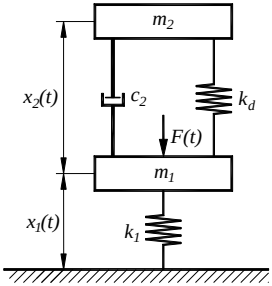

Figure 2.2 Undamped primary system with TMD under harmonic external excitation

The first, applying the complex amplitude method to to solve the system (2.25) and (2.26), then using the fixed-points theory by Den Hartog same as in section 2.1.1, we get the optimal tuning and damping ratios of TMD attached to an undamped primary structure subjected to harmonic external excitation are given in the form, respectively:

$$\beta_{DH} = \frac{1}{1+\mu} \tag{2.10}$$

$$\xi_{DH} = \sqrt{\frac{3\mu}{8(1+\mu)}} \tag{2.11}$$

2.2. Electromechanical coupling model of piezoelectric stack with a tuned mass damper

2.2.1. Modeling of piezoelectric stacks

The structure of a common PSEH is shown in Figure 2.3a, in which the piezoelectric element has *n* layers, each layer has a thickness of h_p, and a total length of $L_p = nh_p$. A PSEH is subjected to an axial force $f_p(t)$, according to the forward piezoelectric effect, which will generate a voltage $V(t)$ on the external resistor R and a charge $q(t)$. In modeling the PSEH, the piezoelectric stack element can be simplified as a compressible elastic bar, the influence of the resistance is small and can be ignored, Figure 2.3b.

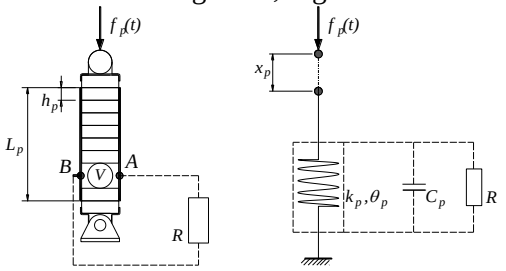

Figure 2.3 The modeling of PSEH: a) structure diagram, b) electromechanical model

The governing equations describing the relationship between the applied force and the electric charge as well as the parameters of the piezoelectric stack assemblies is written as:

$$f_p(t) = k_p x_p(t) + \theta_p V(t) \tag{2.12}$$

$$q(t) = \theta_p x_p(t) - C_p V(t) \tag{2.13}$$

where $$k_p = \frac{c_{33} A}{n h_p}, \theta_p = \frac{e_{33} A}{h_p}, C_p = n \frac{\varepsilon_{33} A}{t_p} \tag{2.14}$$

2.2.2. Modeling of PSEH in series connection with spring

Figure 2.4a describes the mechanical structure of PSEH connected in series with a spring, subjected to the effect of axial force $f(t)$. In which, PSEH has the basic parameters as mentioned in section 2.2.1, the linear spring has stiffness k_s. The deformation of the piezoelectric elements and the spring are x_p and x_s, respectively. The electromechanical model of this PSEH-spring combination connected in series is shown in Figure 2.4b.

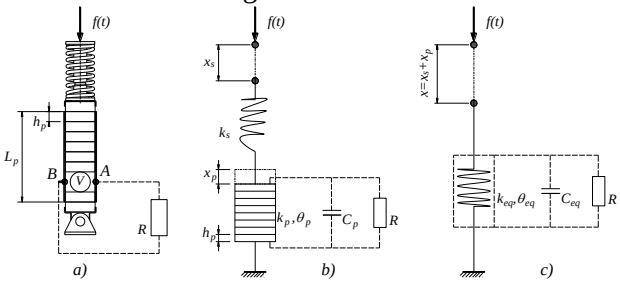

Figure 2.4 The modeling of PSEH in series connection with a spring
a) structure diagram, b) electromechanical model, c) equivalent model.

The governing equations of equivalent PSEH is is written in the form:

$$f = k_{eq} x + \theta_{eq} V \tag{2.15}$$

$$q = \theta_{eq} x - C_{eq} V \tag{2.16}$$

where $$k_{eq} = \frac{k_s k_p}{k_s + k_p}, \theta_{eq} = \frac{k_s}{k_s + k_p} \theta_p, C_{eq} = C_p + \frac{\theta_p^2}{k_s + k_p} \tag{2.17}$$

2.2.3. Modeling of PSEH in parallel connection with spring

Figure 2.5a describes the mechanical structure of the PSEH connected in series with the damper element, subjected to the effect of axial force $f(t)$. In which, the PSEH has the basic parameters as mentioned in section 2.2.1, the linear viscous damper element has a damping coefficient c. The electromechanical model of this series PSEH-damper combination is shown in Figure 2.5b. Mechanically, the PSEH is equivalent to a spring with stiffness k_p,

so this combination is equivalent to a Maxwell element with a connecting node in the middle.

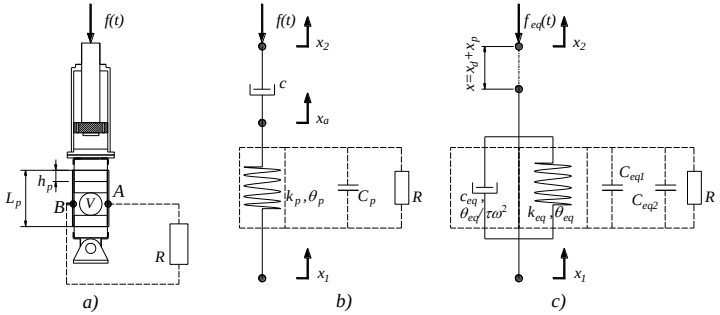

Figure 2.5 The modeling of PSEH in series connection with a damper a) structure diagram, b) electromechanical model, c) equivalent model.

The governing equations of equivalent PSEH is is written in the form:

$$f = k_{eq}\left(x_2 - x_1\right) + c_{eq}\left(\dot{x}_2 - \dot{x}_1\right) + \theta_{eq}V + \frac{\theta_{eq}}{\tau^2\omega^2}\tau\dot{V} \tag{2.18}$$

$$q = \theta_{eq}(x_2 - x_1) + \frac{\theta_{eq}}{\tau^2\omega^2}\tau(\dot{x}_2 - \dot{x}_1) - C_{eq1}V + C_{eq2}\tau\dot{V} \tag{2.19}$$

where

$$\tau = \frac{c}{k_p}, k_{eq} = \frac{\tau^2\omega^2}{1+\tau^2\omega^2}k_p, \theta_{eq} = \frac{\tau^2\omega^2}{1+\tau^2\omega^2}\theta_p,$$
$$c_{eq} = \frac{1}{1+\tau^2\omega^2}c, C_{eq1} = C_p + \frac{1}{1+\tau^2\omega^2}\frac{\theta_p^2}{k_p}, C_{eq2} = \frac{1}{1+\tau^2\omega^2}\frac{\theta_p^2}{k_p} \tag{2.20}$$

2.3. Modeling of PSEH with a force amplification frame

When combining multiple single PSFAF in a main force amplification frame, we will obtain a dual amplification frame called 2sPSFAF (Piezoelectric Stack Energy Harvester and Two-stage Force Amplification Frame) as described in figure 2.6.

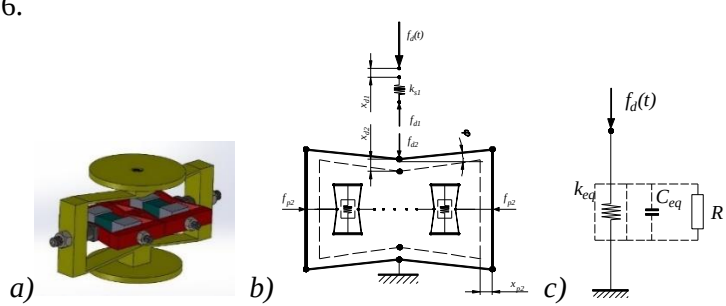

Figure 2.5 The modeling of PSEH with a two-stage force amplification frame a) 3D model, b) physical model, c) equivalent Physical Model.

It can be seen that 2sPSFAF can be modeled as an equivalent PSEH with the following system of equations:

$$f_{d,2} = k_{FAF} x_{d,2} + \theta_{FAF} V \tag{2.21}$$

$$q = \theta_{FAF} x_{d,2} - C_p V \tag{2.22}$$

where $k_{FAF} = \dfrac{k_{p,i}}{N \cot^2(\varphi_i)\cot(\varphi)}, \theta_{FAF} = \dfrac{\theta_{p,i}}{\cot(\varphi_i)\cot(\varphi)}, V = V_p \cot\varphi$ (2.23)

Since 2sPSFAF can be modeled as an equivalent PSEH, its series connection with the spring has stiffness described by the equations:

$$f_d = k_{eq} x_d + \theta_{eq} V \tag{2.24}$$

$$q = \theta_{eq} x_d - C_{eq} V \tag{2.25}$$

where $k_{eq} = \dfrac{k_d k_{FAF}}{k_d + k_{FAF}}, \theta_{eq} = \dfrac{k_d}{k_d + k_{FAF}} \theta_{FAF}, C_{eq} = C_p + \dfrac{\theta_{FAF}^2}{k_d + k_{FAF}}$ (2.26)

The conclusion of chapter 2

In chapter 2, the thesis presents the following issues:

- Den Hartog's fixed point theory as a basis for determining the optimal parameters of TMD.
- Model of tuned mass damper TMD mounted on the undamped primary structure under base and external harmonic excitation. Determination of optimal parameters of the model based on Den Hartog's fixed point theory.
- The model of piezoelectric stack in mechanical systems.
- The integration options of piezoelectric stack assemblies and a two-stage force amplification frame with TMD.

CHAPTER 3. THE OPTIMIZATION DESIGN OF TMD-PSEH BASED ON THE FIXED-POINT THEORY

3.1. TMD-PSEH attached to an undamped primary structure subject to harmonic base excitation.

3.1.1. Response analysis of the system subjected to harmonic base excitation.

Figure 3.1 shows an undamped primary structure with TMD-PSEH subjected to harmonic base excitation. Applying the theoretical basis in section 2.2.1, for the case of a piezoelectric stack assembly connected in series with a spring, the electromechanical equations for the system is written as:

$$f_2 = k_2 x_2 + \theta V \tag{2.27}$$

$$q = \theta x - CV \tag{2.28}$$

where: $k_2 = \dfrac{k_d k_p}{k_d + k_p}, \theta = \dfrac{k_d}{k_d + k_p} \theta_p, C = C_p + \dfrac{\theta_p^2}{k_d + k_p}$ (2.29)

The governing equations for an undamped primary structure with TMD-PSEH subjected to harmonic base excitation are:

$$m_1\ddot{x}_1 - c_2\dot{x}_2 + k_1x_1 - k_2x_2 - \theta V = -m_1\ddot{z} \tag{2.30}$$

$$m_2\ddot{x}_2 + c_2\dot{x}_2 + k_2x_2 + \theta V = -m_2(\ddot{x}_1 + \ddot{z}) \tag{2.31}$$

$$C\dot{V} + \frac{V}{R} = \theta\dot{x}_2 \tag{2.32}$$

By setting:

$$\omega_1 = \sqrt{\frac{k_1}{m_1}}, \omega_2 = \sqrt{\frac{k_2}{m_2}}, \mu = \frac{m_2}{m_1}, \xi_2 = \frac{c_2}{2m_2\omega_2}, \beta = \frac{\omega_2}{\omega_1}, \lambda = \frac{\Omega}{\omega_1},$$
$$\kappa^2 = \frac{\theta^2}{k_2C}, \nu = \frac{CV}{\theta}, \alpha = \frac{1}{\Omega RC} \tag{2.33}$$

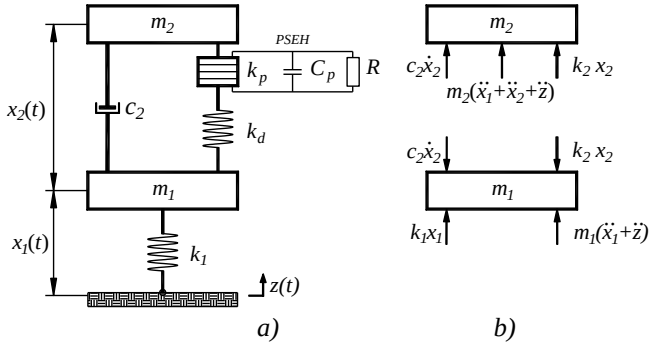

a) *b)*

Figure 3.1 The modeling of an undamped primary structure with TMD-PSEH subjected to harmonic base excitation
a) physical model, b) free-body diagram.

Then the equation system (2.30)–(2.32) is rewritten as:

$$\ddot{x}_1 - 2\mu\omega_1\beta\xi_2\dot{x}_2 + \omega_1^2x_1 - \mu\omega_2^2x_2 - \mu\omega_2^2\kappa^2\nu = -\ddot{z} \tag{2.34}$$

$$\ddot{x}_2 + 2\omega_1\beta\xi_2\dot{x}_2 + \omega_2^2x_2 + \omega_2^2\kappa^2\nu = -\ddot{x}_1 - \ddot{z} \tag{2.35}$$

$$\dot{v} + \alpha\Omega v = \dot{x}_2 \tag{2.36}$$

Applying the complex amplitude method to solve the system of equations, we obtain the magnification factors, voltage amplitude and dimensionless averaging power of the system as follows:

$$K_1 = \frac{a_1}{z_0} = \sqrt{\frac{p_0 + p_1\xi_2 + p_2\xi_2^2}{q_0 + q_1\xi_2 + q_2\xi_2^2}} \tag{2.37}$$

$$\frac{V_0}{z_0} = \frac{\lambda^2}{q_0 + q_1\xi_2 + q_2\xi_2^2} \tag{2.38}$$

$$P_{av} = \frac{\Omega}{2\pi}\int_0^{2\pi/\Omega}\frac{V^2/R}{\omega_1^3m_1z_0^2}dt = \frac{1}{2}\frac{\mu\alpha\beta^2\kappa^2\lambda^5}{q_0 + q_1\xi_2 + q_2\xi_2^2} \tag{2.39}$$

where

$$p_0 = \lambda^4\left(\beta^2(1+\kappa^2)(1+\mu)-\lambda^2\right)^2 + \alpha^2\lambda^4\left(\beta^2(1+\mu)-\lambda^2\right)^2$$
$$p_1 = 4\alpha\kappa\beta^3\lambda^5(1+\mu)^2,\ p_2 = 4\beta^2\lambda^6(1+\alpha^2)(1+\mu)^2$$
$$q_0 = \alpha^2\left(\lambda^2(1-\lambda^2)+\beta^2(\lambda^2(1+\mu)-1)\right)^2 + \left(\lambda^2(1-\lambda^2)+\beta^2(1+\kappa^2)(\lambda^2(1+\mu)-1)\right)^2 \quad (2.40)$$
$$q_1 = 4\alpha\kappa\lambda\beta^3(\lambda^2(1+\mu)-1)^2, q_2 = 4\beta^2\lambda^2(1+\alpha^2)(\lambda^2(1+\mu)-1)^2$$

3.1.2. Optimization of parameters of the system based on fixed-point theory

Generally, two main basic requirements for the effective performance of a TMDPSEH system are technically posted: the first, perhaps also the priority, is to suppress the vibration of the primary structure, the second is to enlarge as much harvested electric energy as possible.

a) The first requirement involves optimizing the stiffness and damping of the TMD-PSEH, represented by the tuning ratio β and damping ratio ξ_2. From this requirement, we apply Den Hartog's fixed point method to determine the optimal parameters β_{op} and ξ_{2op} as follows:

$$\beta_{op} = \beta^*\sqrt{\frac{1+\alpha^2}{1+\alpha^2+\kappa^2}}$$
$$\xi_{2op} = \sqrt{\frac{\xi_{2(1)}^2\big|_{\lambda=\lambda_P} + \xi_{2(2)}^2\big|_{\lambda=\lambda_Q}}{2}} = \xi_{2op}(\alpha,\mu,\kappa^2) \quad (2.41)$$

b) The second requirement involves optimizing the output electrical power. From this requirement, we consider the electric part of PSEH that is represented by a resistor-capacitor parallel circuit, as shown in Eq. (2.36). Neglecting the coupling effect on the circuit, under excitation by a sinusoidal current source with a magnitude I_0 and frequency Ω, the power dissipated by the resistive load R is as follows:

$$P_R = \frac{I_0^2 R}{2\left(1+R^2\Omega^2C^2\right)} \quad (2.42)$$

Solving the condition $\partial P_R / \partial R = 0$ using (2.42), it is found that the circuit has a maximum power output at the optimal resistive load of $R = 1/(\Omega C)$. So, one gets the optimal resistance ratio:

$$\alpha_{op} = 1 \quad (2.43)$$

3.2. TMD-PSEH attached to an undamped primary structure subject to harmonic external excitation.

3.1.1. Response analysis of the system subjected to harmonic external excitation.

Figure 3.2 shows an undamped primary structure with TMD-PSEH subjected to harmonic external excitation $F(\tau)$. The electromechanical equations for the system of the PSEH and TMD series assembly can be deduced from section 2.2.2 as follows:

$$f_2 = k_2 u_2 + \theta V \tag{2.44}$$

$$q = \theta u_2 - CV \tag{2.45}$$

where:
$$k_2 = \frac{k_d k_p}{k_d + k_p}, \theta = \frac{k_d}{k_d + k_p}\theta_p, C = C_p + \frac{\theta_p^2}{k_d + k_p} \tag{2.46}$$

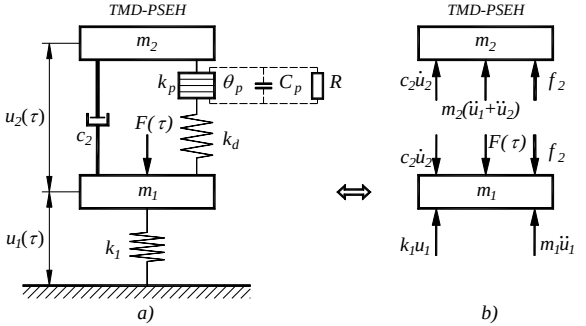

Figure 3.2 The modeling of an undamped primary structure with TMD-PSEH subjected to harmonic external excitation
a) physical model, b) free-body diagram.

The governing equations for an undamped primary structure with TMD-PSEH subjected to harmonic external excitation are:

$$m_1\ddot{u}_1 - c_2\dot{u}_2 + k_1u_1 - k_2u_2 - \theta V = F_0 \cos\Omega\tau \tag{2.47}$$

$$m_2\ddot{u}_2 + c_2\dot{u}_2 + k_2u_2 + \theta V = -m_2\ddot{u}_1 \tag{2.48}$$

$$C\dot{V} + \frac{V}{R} - \theta\dot{u}_2 = 0 \tag{2.49}$$

where the over dots denote the derivatives with respect to time τ. Let us denote:

$$\omega_1 = \sqrt{\frac{k_1}{m_1}}, \omega_2 = \sqrt{\frac{k_2}{m_2}}, \mu = \frac{m_2}{m_1}, \xi_2 = \frac{c_2}{2m_2\omega_2}, \beta = \frac{\omega_2}{\omega_1}, \lambda = \frac{\Omega}{\omega_1},$$
$$\kappa^2 = \frac{\theta^2}{k_2 C}, \nu = \frac{CV}{\theta}, \alpha = \frac{1}{\Omega RC} \tag{2.50}$$

and make the change of variables:

$$t = \omega_1\tau, u_1 = x_1, \dot{u}_1 = \omega_1\dot{x}_1, \ddot{u}_1 = \omega_1^2\ddot{x}_1, u_2 = x_2, \dot{u}_2 = \omega_1\dot{x}_2, \ddot{u}_2 = \omega_1^2\ddot{x}_2 \tag{2.51}$$

Then the equation system (2.47)-(2.49) can be transformed into the following dimensionless system:

$$\ddot{x}_1 - 2\mu\beta\xi_2\dot{x}_2 + x_1 - \mu\beta^2 x_2 - \mu\beta^2\kappa^2\nu = X_{st}\cos\lambda t \tag{2.52}$$

$$\ddot{x}_2 + 2\beta\xi_2\dot{x}_2 + \beta^2 x_2 + \beta^2\kappa^2 v = -\ddot{x}_1 \tag{2.53}$$

$$\dot{v} + \lambda\alpha v = \dot{x}_2 \tag{2.54}$$

where the over dots now denote the derivatives with respect to dimensionless time t, X_{st} is the static deflection of the primary structure.

$$X_{st} = F_0 / k_1 \tag{2.55}$$

Applying the complex amplitude method to solve the system of equations, we obtain the magnification factors and voltage amplitude of the system as follows:

$$K_1 = \frac{a_1}{X_{st}} = \sqrt{\frac{p_0 + p_1\xi_2 + p_2\xi_2^2}{q_0 + q_1\xi_2 + q_2\xi_2^2}} \tag{2.56}$$

$$K_2 = \frac{a_2}{X_{st}} = \lambda^2\sqrt{\frac{1+\alpha^2}{q_0 + q_1\xi_2 + q_2\xi_2^2}} \tag{2.57}$$

$$V_0 = X_{st}v_0, v_0 = \frac{\lambda^2}{\sqrt{q_0 + q_1\xi_2 + q_2\xi_2^2}} \tag{2.58}$$

where

$$\begin{gathered} p_0 = [\beta^2(1+\kappa^2) - \lambda^2]^2 + \alpha^2(\beta^2 - \lambda^2)^2, p_1 = 4\alpha\kappa^2\lambda\beta^3, p_2 = 4\lambda^2\beta^2(1+\alpha^2), \\ q_0 = \left\{(\lambda^2 - 1)[\beta^2(1+\kappa^2) - \lambda^2] + \mu\lambda^2\beta^2(1+\kappa^2)\right\}^2 + \\ +\alpha^2\left[(\lambda^2 - 1)(\beta^2 - \lambda^2) + \mu\lambda^2\beta^2\right]^2, \\ q_1 = 4\alpha\kappa^2\lambda\beta^3\left[\lambda^2(1+\mu) - 1\right]^2, q_2 = 4\lambda^2\beta^2(1+\alpha^2)\left[\lambda^2(1+\mu) - 1\right]^2 \end{gathered} \tag{2.59}$$

3.2.2. ***Optimization of parameters of the system based on fixed-point theory***

Generally, two main basic requirements for the effective performance of a TMDPSEH system are technically posted: the first, perhaps also the priority, is to suppress the vibration of the primary structure, the second is to enlarge as much harvested electric energy as possible.

a) The first requirement involves optimizing the stiffness and damping of the TMD-PSEH, represented by the tuning ratio β and damping ratio ξ_2.

b) The second requirement involves optimizing the output electrical power.

Using the same method as section 3.1.2, we determine the optimal parameters:

$$\beta_{op} = \beta_{DH}\sqrt{\frac{1+\alpha^2}{1+\alpha^2+\kappa^2}} \tag{2.60}$$

$$\xi_{2op} = \sqrt{\frac{\xi_{2(1)}^2\big|_{\lambda=\lambda_P} + \xi_{2(2)}^2\big|_{\lambda=\lambda_Q}}{2}} = \xi_{2op}(\alpha, \mu, \kappa^2) \tag{2.61}$$

$$\alpha_{op} = 1 \tag{2.62}$$

3.3. TMD-PSEH with a force amplification frame attached to an undamped primary structure subject to harmonic external excitation.

3.3.1. Response analysis of the system

The proposed system in the Patent deals with a TMD incorporating a 2sPSFAF (TMD-2sPSFAF) which is depicted in Fig. 3.3a. The primary structure has a mass and a linear spring of stiffness , it is undamped and subjected to harmonic external excitation $F(\bar{t})$

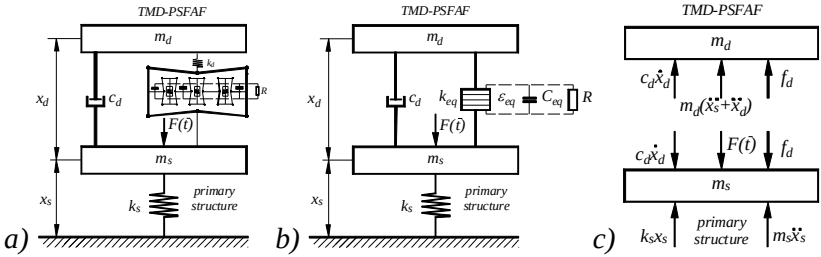

Figure 3.3 The modeling of an undamped primary structure with TMD-2sPSFAF subjected to harmonic external excitation
a) physical model, b) equivalent model, c) free-body diagram.

The governing equations of the considered system are given by:

$$\begin{aligned} &m_1\ddot{x}_1 - c_2\dot{x}_2 + k_1x_1 - k_{eq}x_2 - \theta_{eq}V = F_0\cos(\Omega\bar{t}) \\ &m_2\ddot{x}_2 + c_2\dot{x}_2 + k_{eq}x_2 + \theta_{eq}V = -m_2\ddot{x}_1 \\ &C_{eq}\dot{V} + \frac{V}{R} = \theta_{eq}\dot{x}_d \end{aligned} \tag{2.63}$$

By setting:

$$\begin{aligned} &t = \omega_s\bar{t}, x_s = x_1, x_d = x_2, \omega_s = \sqrt{k_s / m_s}, \omega_d = \sqrt{k_{eq} / m_d}, \mu = m_d / m_s, \\ &\xi_d = \frac{c_d}{2m_d\omega_d}, \beta = \frac{\omega_d}{\omega_s}, \lambda = \frac{\omega}{\omega_s}, \kappa^2 = \frac{\theta_{eq}^2}{k_{eq}C_{eq}}, \nu = \frac{C_{eq}V}{\theta_{eq}}, \alpha = \frac{1}{\omega RC_{eq}}, X_{st} = \frac{F_0}{k_s} \end{aligned} \tag{2.64}$$

The equation system (2.63) can be transformed into the following dimensionless system:

$$\begin{aligned} &\ddot{x}_1 - 2\mu\beta\xi_2\dot{x}_2 + x_1 - \mu\beta^2x_2 - \mu\beta^2\kappa^2\nu = X_{st}\cos\lambda t \\ &\ddot{x}_2 + 2\beta\xi_2\dot{x}_2 + \beta^2x_2 + \beta^2\kappa^2\nu = -\ddot{x}_1 \\ &\dot{\nu} + \lambda\alpha\nu = \dot{x}_2 \end{aligned} \tag{2.65}$$

Applying the complex amplitude method to solve the system of equations, we obtain the magnification factors K_1, K_2 and voltage amplitude ν_0 as follows:

$$K_1 = \frac{A_1}{X_{st}} = \sqrt{\frac{B_1^2 + B_2^2}{E_1^2 + E_2^2}} \tag{2.66}$$

$$K_2 = \frac{A_2}{X_{st}} = \sqrt{\frac{C_1^2 + C_2^2}{E_1^2 + E_2^2}} \tag{2.67}$$

$$v_0 = \frac{A_3}{X_{st}} = \sqrt{\frac{D_1^2 + D_2^2}{E_1^2 + E_2^2}} \tag{2.68}$$

3.3.2. Determination of the system parameters

To investigate the undamped primary structure with TMD-2sPSFAF in considering $\kappa^2 \to 0$, the results of the optimal mechanical TMD obtained by the fixed point theory in section 2.1.2 are adopted for β and of TMD-2sPSFAF:

$$\beta = \beta_{DH} = \frac{1}{1+\mu} \tag{2.69}$$

$$\xi_2 = \xi_{DH} = \sqrt{\frac{3\mu}{8(1+\mu)}} \tag{2.70}$$

From (2.69) one has:

$$k_{eq} = \frac{\mu}{(1+\mu)^2} k_1 \tag{2.71}$$

Substituting (2.71) into the first equation in (2.26), one gets:

$$k_d = \frac{\mu k_s k_{p,i}}{(1+\mu)^2 k_{p,i} - \mu N \cot^2(\varphi_i)\cot(\varphi) k_s} \tag{2.72}$$

The conclusion of chapter 3

Based on the theoretical basis in chapter 2, the thesis presented the issues in chapter 3 as follows:

- Building a physical model and establishing the corresponding differential equations for the electromechanical system including the undamped primary structure integrated TMD-PSEH subjected to base excitation and external excitation.

- Based on the two main technical requirements of eliminating vibrations of the primary structure and increasing the energy harvesting capacity, the coefficients such as tuning ratio β_{op}, damping ratio $\xi_{2\text{op}}$ and resistance ratio α_{op} were determined by analytical method.

- In the final part, a model of a piezoelectric stack energy harvester mounted in a two-stage force amplification frame 2sPSFAF was built. Then, the governing equations of the system was established to determine the electromechanical responses by the complex amplitude method.

CHAPTER 4. POWER FLOW ANALYSIS OF TMD-PSEH SYSTEM AND NUMERICAL EXAMINATION

4.1. Distributions of power flow and efficiency of TMD-PSEH

4.1.1. Distributions of power flow

In the model considered in Figure 3.2, an equivalent resistive load is used to represent the entire harvesting electrical module and to provide an estimation of the harvesting electrical energy obtained.

The energy per cycle is defined as the integral of power over a period as follows:

$$\begin{aligned} \bar{E}_{\text{in}} &= \bar{E}_d + \bar{E}_{\text{out}} \\ \Leftrightarrow \pi K_1 \left|-\sin\varphi_1\right| &= 2\pi\mu\lambda\beta\xi_2 K_2^2 + \pi\mu\beta^2\kappa^2\alpha v_0^2 \end{aligned} \tag{2.73}$$

where

$$\bar{E}_{\text{in}} = X_{\text{st}} \int_0^{2\pi/\lambda} \cos\lambda t\left[-\lambda a_1 \sin(\lambda t+\varphi_1)\right] dt = \pi X_{\text{st}} a_1 \left|-\sin\varphi_1\right| = \pi \left|-\sin\varphi_1\right| K_1 X_{\text{st}}^2,$$

$$\bar{\Pi}_1 = \frac{\left[-\lambda a_1 \sin(\lambda t+\varphi_1)\right]^2}{2}\Big|_0^{\frac{2\pi}{\lambda}} = 0, \bar{\Pi}_2 = \frac{\mu\lambda^2\left[-a_1\sin(\lambda t+\varphi_1) - a_2\sin(\lambda t+\varphi_2)\right]^2}{2}\Big|_0^{\frac{2\pi}{\lambda}} = 0,$$

$$\bar{U}_1 = \frac{\left[a_1\cos(\lambda t+\varphi_1)\right]^2}{2}\Big|_0^{\frac{2\pi}{\lambda}} = 0, \bar{U}_2 = \frac{\mu\beta^2\left[a_2\cos(\lambda t+\varphi_2)\right]^2}{2}\Big|_0^{\frac{2\pi}{\lambda}} = 0,$$

$$\bar{E}_C = \frac{\mu\beta^2\kappa^2\left[V_0\cos(\lambda t+\varphi_v)\right]^2}{2}\Big|_0^{\frac{2\pi}{\lambda}} = 0,$$

$$\bar{E}_d = 2\mu\beta\xi_2 \int_0^{2\pi/\lambda} \left[-\lambda a_2 \sin(\lambda t+\varphi_2)\right]^2 dt = 2\pi\mu\lambda\beta\xi_2 a_2^2 = 2\pi\mu\lambda\beta\xi_2 K_2^2 X_{\text{st}}^2$$

$$\bar{E}_{\text{out}} = \mu\beta^2\kappa^2\lambda\alpha \int_0^{2\pi/\lambda} \left[V_0\cos(\lambda t+\varphi_v)\right]^2 dt = \pi\mu\beta^2\kappa^2\alpha V_0^2 = \pi\mu\beta^2\kappa^2\alpha v_0^2 X_{\text{st}}^2$$

4.1.2. Average input and output powers, and efficiency

The average power as the average amount of energy performed per cycle. From that we can determine:

$$\bar{P}_{\text{in}} = \frac{\bar{E}_{\text{in}}}{2\pi/\lambda} = \frac{\lambda\left|-\sin\varphi_1\right| X_{\text{st}}^2}{2} K_1 = \frac{\lambda\left|-\sin\varphi_1\right| X_{\text{st}}^2}{2} \sqrt{\frac{p_0 + p_1\xi_2 + p_2\xi_2^2}{q_0 + q_1\xi_2 + q_2\xi_2^2}} \tag{2.74}$$

$$\bar{P}_d = \frac{\bar{E}_d}{2\pi/\lambda} = \lambda^2\mu\beta\xi_2 X_{\text{st}}^2 K_2^2 = \lambda^4\mu\beta X_{\text{st}}^2 \frac{(1+\alpha^2)\xi_2}{q_0 + q_1\xi_2 + q_2\xi_2^2} \tag{2.75}$$

$$\bar{P}_{\text{out}} = \frac{\bar{E}_{\text{out}}}{2\pi/\lambda} = \frac{\mu\beta^2\kappa^2\alpha\lambda X_{\text{st}}^2}{2} v_0^2 = \frac{\mu\alpha\beta^2\kappa^2\lambda^5 X_{\text{st}}^2}{2(q_0 + q_1\xi_2 + q_2\xi_2^2)} \tag{2.76}$$

The efficiency of mechanical-electrical conversion can be calculated by the ratio of average output and input powers. Therefore, the efficiency formulation for the PSEH system is as follows:

$$\eta = \frac{\mu\beta^2\kappa^2\alpha}{\left|-\sin\varphi_1\right|}\frac{v_0^2}{K_1} = \frac{\mu\alpha\beta^2\kappa^2\lambda^4}{\left|-\sin\varphi_1\right|\sqrt{\left(p_0+p_1\xi_2+p_2\xi_2^2\right)\left(q_0+q_1\xi_2+q_2\xi_2^2\right)}} \tag{2.77}$$

4.2. Numerical examination of TMD-PSEH attached to an undamped primary structure subject to harmonic base excitation

Here, a numerical examination of the undamped primary structure with the TMD-PSEH is carried out with:

$$\mu = 0.05,\ \kappa^2 = 0.05,\ \alpha = \alpha_{op} = 1,\ \beta = \beta_{op}$$

Figure 4.1a depicts curves $K_1(\lambda)$ with five values of ξ_2. Clearly, the curve related to $\xi_2 = \xi_{2op}$ has the lowest peaks in comparison with the curves related to four other values of ξ_2. Figure 4.1b depicts four curves $K_1(\lambda)$ with $\xi_2 = \xi_{2op}$ and five values of α. This case corresponds to adjusting the external resistor R for the optimal TMD-PSEH in use.

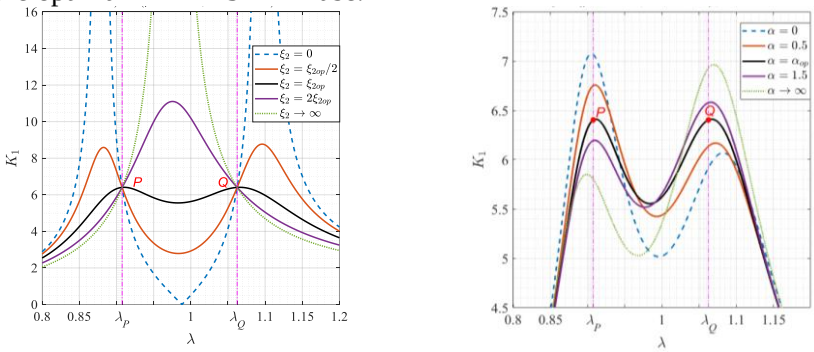

a) *b)*

Figure 4.1 $K_1(\lambda)$ *with: a)* $\alpha = \alpha_{op}$, ξ_2 *varies, b)* $\xi_2 = \xi_{2op}$, α *varies*

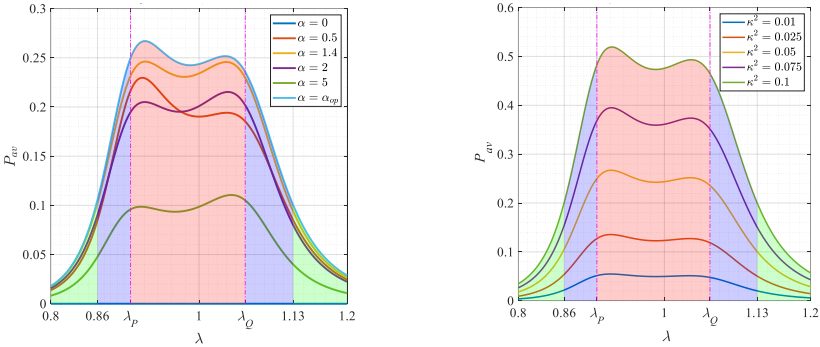

a) *b)*

Figure 4.2 P_{av} *with: a)* $\kappa^2 = 0.05$, α *varies, b)* $\alpha = \alpha_{op}$, κ^2 *varies*

Hình 4.2a depicts the average output power $P_{av}(\lambda)$ of TMD-PSEH with β_{op}, ξ_{2op} and α varies. Clearly, the curve related to $\alpha = 1$ is the enveloped curve and shows the largest amount of electrical harvest energy in a period. Hình 4.2a depicts $P_{av}(\lambda)$ of optimal TMD-PSEH with the variations of κ^2. Obviously, the higher the value of κ^2, the larger the value of P_{av}.

4.3. Numerical examination of TMD-PSEH attached to an undamped primary structure subject to harmonic external excitation

In this section, we carry out a numerical investigation of the undamped primary structure-TMD-PSEH system. Initial input parameters are taken so that $\mu = 0.05, \kappa^2 = 0.05$.

Figure 4.3a and 4.3b depict magnification factors $K_1(\lambda), K_2(\lambda)$. It is seen that the curve K_1 has two fixed points $P(\lambda_P, K_{1P}), Q(\lambda_Q, K_{1Q})$ independent of damping, while the curve K_2 also has a fixed point $S(\lambda_S, K_{2S})$. The optimal tuning and damping ratios β_{op} and ξ_{2op} keep the two peaks of equal magnitude of the curve K_1 always lower when compared to that involving non-optimal values.

Besides, in comparison with the same undamped primary structure with the optimal mechanical TMD (namely, $\kappa^2 = 0, \beta_{op} = \beta_{\mathrm{DH}}, \xi_{2op} = \xi_{DH}$ while the other parameters are fixed) as illustrated in Figure 4.c và Figure 4.d, it is seen that the curves K_1 and K_2 related to a TMD-PSEH differ from the curves K_1 and K_2 related to a mechanical TMD for non-optimal values of β and ξ_2.

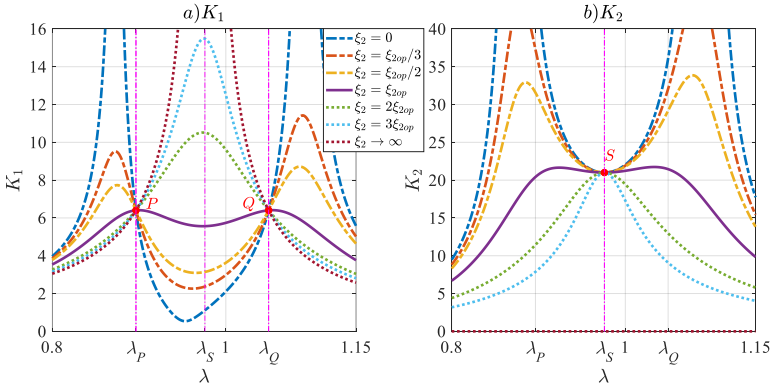

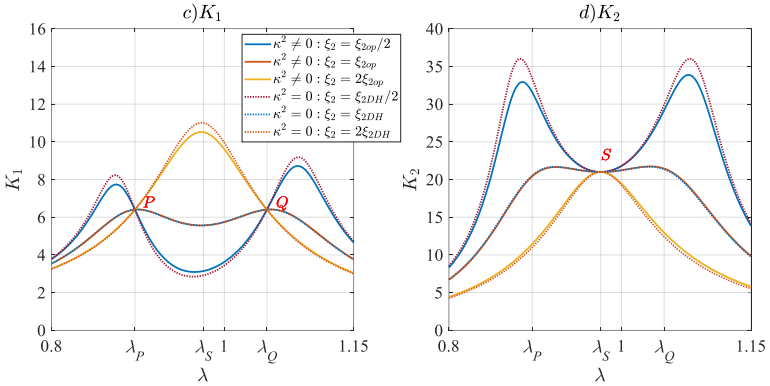

Figure 4.3 K_1, K_2 *versus with* $\mu = 0.05, \alpha = \alpha_{op}$ *and* ξ_2 *varies*

a) $K_1(\kappa^2 = 0.05)$, *b)* $K_2(\kappa^2 = 0.05)$, *c)* $K_1(\kappa^2 = 0)$,*d)* $K_2(\kappa^2 = 0)$

Figure 4.4 and Figure 4.5 show the effects of piezoelectric and electrical parameters κ^2 and α on K_1 and K_2 along with the frequency axis. In Figure 4.4, the values of μ, α are unchanged, but the values of β_{op} and ξ_{2op} are considered to vary with κ^2. In other words, different piezoelectric material relates to different optimal tuning and damping ratios. Although the variations of κ^2 have little effect on both K_1 and K_2 in amplitude due to its small value, it is remarkable that K_1 has two fixed points independent of κ^2 and K_2 also has such a fixed point, which is exactly $P(\lambda_P, K_{1P}), Q(\lambda_Q, K_{1Q})$ and $S(\lambda_S, K_{2S})$, respectively.

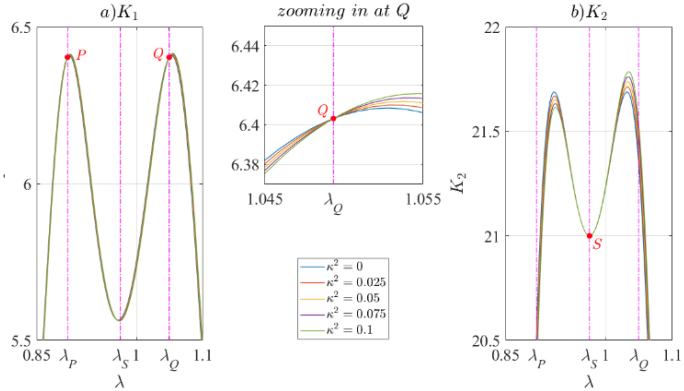

Figure 4.4 K_1, K_2 *versus with* $\mu = 0.05, \alpha = \alpha_{op}$ *and* κ^2 *varies*

a) K_1, *b)* K_2

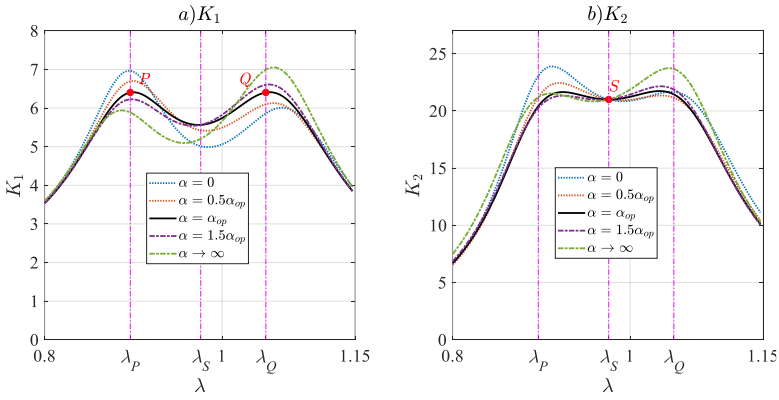

Figure 4.5 K_1, K_2 *versus with* $\mu = 0.05, \kappa^2 = 0.05$ *and* α *varies*
a) K_1, *b)* K_2

In the Figure 4.5, the values of μ, κ^2 are unchanged, also the values of β_{op} and $\xi_{2\text{op}}$ change according to α. It is easy to see that, any change in the value of α deviating from α_{op} leads to one of the two peaks of K_1, K_2 being higher than the other.

Figure 4.6a shows the time histories of dimensionless responses of mechanical displacements and voltage at the frequency ratio $\lambda = [1, \lambda_P]$. The responses are sinusoidal with the period of $2\pi / \lambda$. Figure 4.6b shows the phase angles between x1, x2, v and the excitation at different frequency ratios for two critical values of the resistance ratio $\alpha = [0, \alpha_{\text{op}}]$. Through the graph we see that, there is always a large phase difference between x1 and x2. Such a phase difference produces a large energy dissipation contributed by the TMD-PSEH inertia force.

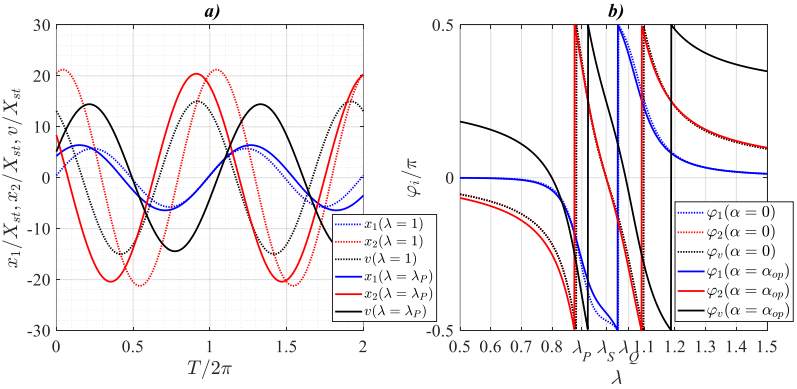

Figure 4.6 Displacement and voltage responses
a) Time histories, b) Phases versus frequency

4.4. Numerical examination of power flow and efficiency

Figure 4.7 depicts dimensionless voltage amplitude v_0 as well as the average powers along with the frequency axis, $\overline{P}_{\text{in}}, \overline{P}_d, \overline{P}_{\text{out}}$. It is clear that v_0 and $\overline{P}_{\text{out}}$ có have a fixed point independent of damping at $\lambda = \lambda_S$, while $\overline{P}_{\text{in}}$ và $\overline{P}_d$ ave no such a fixed point. Like the curve K_2, both curves $v_0, \overline{P}_{\text{out}}$ related to $\xi_2 = \xi_{2\text{op}}$ đều have two peaks of quite similar height appearing in the vicinity of λ_P, λ_Q. Meanwhile, the curves $\overline{P}_{\text{in}}$ và $\overline{P}_d$ also have two peaks occurring around λ_P, λ_Q. It is noted that at critical values of ξ_2 is $v_0 \to \infty, \overline{P}_{\text{in}} \to \infty, \overline{P}_d = 0, \overline{P}_{\text{out}} \to \infty$ khi $\xi_2 \to 0$ và $v_0 = \overline{P}_d = \overline{P}_{\text{out}}$ as $\xi_2 \to \infty$ since the two vibration masses are "interlocked". Therefore, this shows again that it is not possible to increase the electrical harvesting power by reducing damping too small because it conflicts with the priority requirement of vibration suppression for the primary structure.

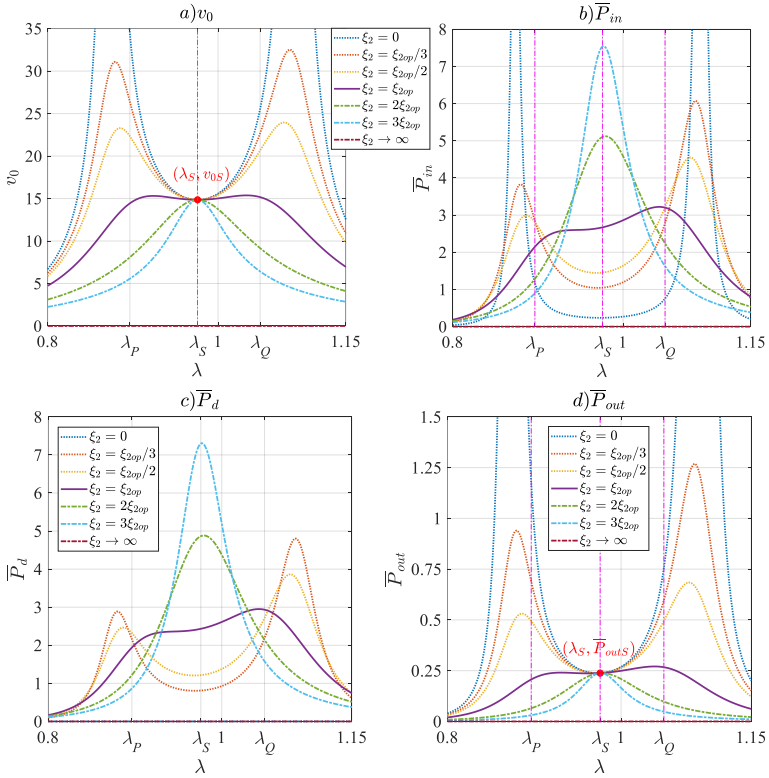

Figure 4.7 Voltage amplitude and average powers per cycle versus λ with $\mu = 0.05, \kappa^2 = 0.05, \alpha = \alpha_{\text{op}}, X_{\text{st}}^2 = 1$ and ξ_2 varies

a) v_0, b) $\overline{P}_{\text{in}}$, c) $\overline{P}_d$, d) $\overline{P}_{\text{out}}$

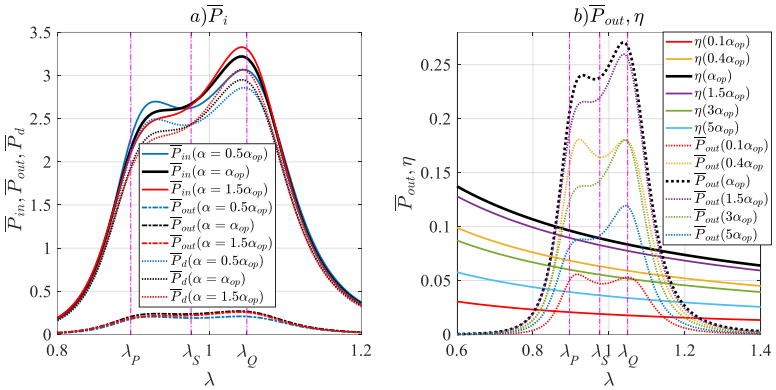

Figure 4.8 Average powers and efficiency versus λ *with* $\kappa^2 = 0.05, \mu = 0.05, X_{st}^2 = 1$ *and* α *varies*

a) $\overline{P}_{in}, \overline{P}_d, \overline{P}_{out}$ *, b)* $\overline{P}_{out}, \eta$

Figure 4.8a depicts average powers $\overline{P}_{in}, \overline{P}_d, \overline{P}_{out}$ per cycle versus frequency with the variation of α. All average power curves have two peaks whereas the right peak of $\overline{P}_{in}, \overline{P}_d$ near λ_Q is always higher than the left one near λ_P.

Figure 4.8b illustrates the correlation between the average output power $\overline{P}_{out}$ and the efficiency η with various values of α in the frequency domain. The left and right peaks of $\overline{P}_{out}$ are equal as $\alpha = 0.4\alpha_{op}$. It can be seen that small values of α reduce the power $\overline{P}_{out}$ very quickly than large values. The closer the value of α is to , the higher the electrical power obtained. Clearly, $\overline{P}_{out}(\alpha = \alpha_{op})$ is the enveloped curve.

Any change in the value of α deviating from α_{op} leads to a decrease of η. Nevertheless, the efficiency is quite low, even in the resonance region the maximum value is only about 10%. Besides, the efficiency η is a decreasing function along with the frequency. As we can see in Figure 4.8a, most of the vibrational energy is transferred to the dissipated energy to reduce the vibration, and the rest is converted to electrical energy which accounts for a small portion. In other words, the dissipated energy is close to the input energy as the frequency increases, resulting in a decrease in efficiency.

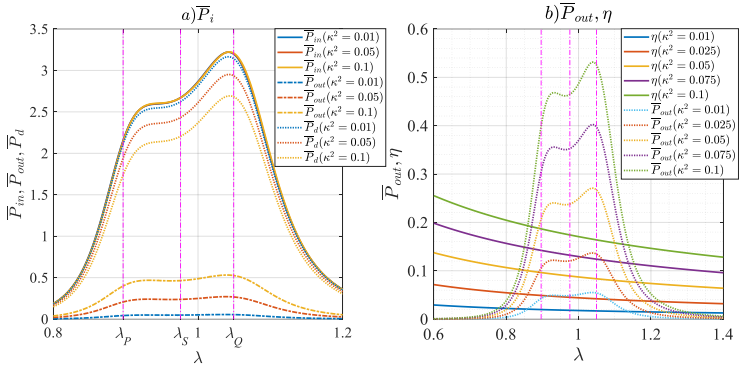

Figure 4.9 Average powers and efficiency versus λ with $\mu=0.05,\alpha=\alpha_{\text{op}},X_{\text{st}}^2=1$ and κ^2 varies

a) $\overline{P}_{\text{in}},\overline{P}_d,\overline{P}_{\text{out}}$, b) $\overline{P}_{\text{out}},\eta$

The effect of the electromechanical coupling coefficient κ^2 on the $\overline{P}_{\text{in}},\overline{P}_d,\overline{P}_{\text{out}}$ and η is illustrated in Figure 4.9. One can see from Figure 4.9 that the effect of κ^2 on $\overline{P}_{\text{in}}$ can be negligible but is significant on $\overline{P}_d,\overline{P}_{\text{out}}$. As κ^2 gets larger, the curve $\overline{P}_d$ is further away from the curve $\overline{P}_{\text{out}}$ and vice versa. As shown in Figure 4.9b, the larger the value of κ^2, the higher the peak and the wider the coverage of the curve $\overline{P}_{\text{out}}$ will be. $\overline{P}_{\text{out}}$ is almost linearly proportional to κ^2 and the variation of η with respect to κ^2 is similar. Physically, it is clear that the better electromechanical coupling, the higher the electrical power.

4.5. Numerical examination of TMD-2sPSFAF attached to an undamped primary structure subject to harmonic external excitation

In this section, we carry out a numerical investigation of the undamped primary structure-TMD-2sPSFAF system.

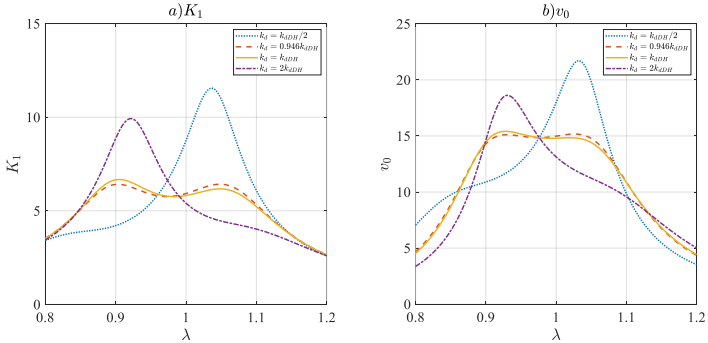

Figure 4.10 K_1,v_0 versus λ with $\mu=0.05,\kappa^2=0.0242,\alpha=1$ and k_d varies

a) K_1, b) v_0

Figures 4.10a and 4.10b depict the curves of the mechanical magnification factor K_1 and the voltage amplitude factor v_0 in the frequency domain λ with k_d varies.

In the figure 4.10a, it is seen that the curve K_1 always has two peaks, however, it is not optimized due to the heights of those two peaks are not equal in the case $k_d = k_{dDH}/2$, $k_d = k_{dDH}$, và $k_d = 2k_{dDH}$. Meanwhile, we can optimize K_1 by changing the value of k_d empirically, say $k_d = 0.946k_{dDH}$ that is a little smaller than k_{dDH}

At the first glance, the curve v_0 has the same properties as that of the curve K_1, as shown in figure 4.10b. With the value $k_d = 0.946k_{dDH}$, the curve is almost optimized. Furthermore, it is seen that the curve has a fixed point independent of the TMD spring stiffness k_d. Therefore, one can see a good matching between the mechanical domain and the electrical one with the effective value of k_d, i.e. $k_d = 0.946k_{dDH}$.

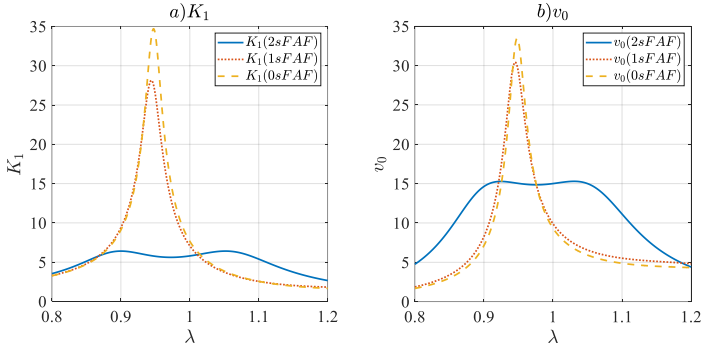

Figure 4.11 K_1, v_0 versus λ with $\mu = 0.05, \kappa^2 = 0.0242, \alpha = 1$ and $k_d = 0.946k_{dDH}$ in different cases
a) K_1, b) v_0

The graph in figure 4.11a makes it clear that there are differences in the TMD spring's equivalent stiffness between the three scenarios, namely $k_{eq-PSEH} = 4.292 > k_{eq-1sFAF} = 4.025 > k_{eq-2sPSFAF} = 2.622$. As the result, installing an FAF lessens the TMD spring's stiffness, improving the system's ability to lessen vibrations. The TMD-2sPSFAF provides the best results in terms of spring stiffness. Furthermore, we can observe from figure 4.11b that among the three scenarios, the voltage amplitude of TMD-2sPSFAF is the least. Nonetheless, the mechanical gain parameter K1 will take precedence in the TMD design problem, making the TMD-2sPSFAF scenario the best option.

The conclusion of chapter 4

In chapter 4, the thesis conducted energy flow analysis and numerical examination to evaluate the theoretical analysis results performed in chapter 3. The numerical examination showed that:

- The system of an undamped primary structure with TMD-PSEH demonstrates a very good agreement between theory and calculation. The two peaks of the curve $K_1(\lambda)$ are very close to P and Q and have almost equal coordinates, resulting in the largest amount of collected power $\bar{P}_{\text{out}}$ in one cycle and the highest efficiency η with the obtained optimal parameters.

- The system of an undamped primary structure with TMD-PSEH and with TMD both provides good vibration suppression for the main structure, provided that the optimal natural frequency ratio coefficients and damping coefficients are derived from fixed point theory.

- In addition, the electromechanical system of TMD-2sPSFAF shows that the voltage amplitude curve has a fixed point that is unaffected by the stiffness of the TMD spring. In addition, the TMD spring's effective stiffness would be determined to guarantee that the voltage amplitude and mechanical magnification curve peaks are at the same heights.

CONCLUSIONS AND FUTURE WORK

CONCLUSIONS

This thesis studies the tuned mass damper TMD integrated with a piezoelectric stack energy harvester PSEH mounted on the undamped primary structure under harmonic excitation and has achieved the following main results:

- First, based on the two main technical requirements of eliminating vibration of the main structure and increasing the electric energy collection capacity, together with Den Hartog's fixed point theory, it helps to determine the optimal parameters of TMD-PSEH such as tuning ratio β_{op}, damping ratio $\xi_{2\text{op}}$ and resistance ratio α_{op}.

- Next, the study of mechanical-mechanical and electromechanical energy conversion was conducted through power/energy flow analysis which showed that in one oscillation cycle, a part of the vibration suppression ability comes from the energy dissipation ability of the TMD, the rest comes from the energy dissipation ability of the PSEH and is converted into electrical energy by the resistor R.

- In addition, a model of a stacked piezoelectric energy harvester mounted in a two-stage force amplification frame 2sPSFAF integrated on the undamped primary structure subjected to external excitation was also studied. The electromechanical system of the TMD-2sPSFAF showed good vibration

reduction ability for the primary structure but also led to a significant reduction in the harvestedvoltage.

- Finally, it can be seen that the fixed point theory has great potential for research application to TMD systems that harvest energy from vibration.

FUTURE WORK

Based on the research results obtained in this thesis, it can lead to the future work following:

- The model of a piezoelectric stack installed in series with the damper element of TMD, or installed in series with both the damper and the spring, or between 2 springs, or located between the damper and the spring;
- The model of a piezoelectric stack installed in series with the spring of the primary structure, or installed in series with both the springs of the primary structure and TMD;
- The model of TMD with the damped primary structure;
- The model of TMD with nonlinear spring or nonlinear damper;
- The model of TMD installed on the primary structure with nonlinear spring.

LIST OF THE PUBLICATIONS RELATED TO THE DISSERTATION

1. **Vũ Anh Tuấn**, Tống Đức Năng, Nguyễn Ngọc Linh, Vũ Đức Lập. *Nghiên cứu thiết bị giảm chấn khối lượng tích hợp bộ thu thập năng lượng kiểu xếp chồng*. Tạp chí Cơ khí Việt Nam, số đặc biệt 11/2022. Trang 316.

2. N.N.Linh, **V.A.Tuan**, N.V.Man, N.D.Anh. *Response analysis of undamped primary system subjected to base excitation with a dynamic vibration absorber intergrated with a piezoelectric stack energy harvester*. Vietnam Journal of Mechanics. Vol 44, No. 4 (2022), pp. 490-499.

3. **Vu Anh Tuan**, N.N.Linh, Nguyen Van Manh, Pham Manh Thang, N.D.Anh. *Investigation of a tuned mass damper with piezoelectric stack energy harvester attached to an undamped primary structure under harmonic base excitation.* Lecture Notes in Civil Engineering, 460 (2024), pp 283–293.

4. N.D.Anh, **Vu Anh Tuan**, Pham Manh Thang, N.N.Linh. *Extension of the fixed point theory to tuned mass dampers with piezoelectric stack energy harvester.* Journal of Sound and Vibration 581 (2024), 118411.

5. NN Linh, ND Anh, LD Viet, NA Ngoc, **VA Tuan**, TD Nang, NV Manh, Sáng chế: *Thiết bị tắt chấn động lực tích hợp bộ thu thập năng lượng dao động kiểu áp điện*, Cục sở hữu trí tuệ - Bộ Khoa học và Công nghệ, Bằng độc quyền sáng chế số 39054, 26/7/2022.

6. Anh Ngoc Nguyen, Duc Nang Tong, **Anh Tuan Vu**, Dong Anh Nguyen, Duc Viet La, Tuan Anh Tran and Ngoc Linh Nguyen. *A design of tuned mass damper with piezoelectric stack energy harvester and two-stage force amplification frame*, Vietnam Journal of Mechanics, 2024. https://doi.org/10.15625/0866-7136/21026.